

CONSTRAINING LOW-FREQUENCY ALFVÉNIC TURBULENCE IN THE SOLAR WIND USING DENSITY-FLUCTUATION MEASUREMENTS

BENJAMIN D. G. CHANDRAN¹, ELIOT QUATAERT², GREGORY G. HOWES³, QIAN XIA¹, AND PEERA PONGKITIWANICHAKUL¹

¹ Space Science Center and Department of Physics, University of New Hampshire, Durham, NH, USA;

benjamin.chandran@unh.edu, qdy2@cisunix.unh.edu, pbu3@cisunix.unh.edu

² Astronomy Department & Theoretical Astrophysics Center, 601 Campbell Hall, University of California, Berkeley, CA 94720, USA; eliot@astro.berkeley.edu

³ Department of Physics and Astronomy, University of Iowa, Iowa City, IA, USA; gregory-howes@uiowa.edu

Received 2009 August 5; accepted 2009 November 4; published 2009 December 7

ABSTRACT

One proposed mechanism for heating the solar wind, from close to the Sun to beyond ~ 10 AU, invokes low-frequency, oblique, Alfvén-wave turbulence. Because small-scale oblique Alfvén waves (kinetic Alfvén waves, KAWs) are compressive, the measured density fluctuations in the solar wind place an upper limit on the amplitude of KAWs and hence an upper limit on the rate at which the solar wind can be heated by low-frequency, Alfvénic turbulence. We evaluate this upper limit for both coronal holes at $5 R_{\odot}$ and the near-Earth solar wind. At both locations, the upper limit we find is consistent with models in which the solar wind is heated by low-frequency Alfvénic turbulence. At 1 AU, the upper limit on the turbulent heating rate derived from the measured density fluctuations is within a factor of 2 of the measured solar-wind heating rate. Thus, if low-frequency Alfvénic turbulence is the primary mechanism for heating the near-Earth solar wind, KAWs must be one of the dominant sources of solar-wind density fluctuations at frequencies ~ 1 Hz. We also present a simple argument for why density-fluctuation measurements do appear to rule out models in which coronal holes are heated by non-turbulent high-frequency waves (“sweeping”), but are compatible with heating by low-frequency Alfvénic turbulence.

Key words: MHD – solar wind – Sun: corona – turbulence – waves

1. INTRODUCTION

A number of observations indicate that the solar wind undergoes spatially extended heating. For example, in situ measurements from satellites such as *Helios* & *Voyager* show that electrons and protons have non-adiabatic temperature profiles at heliocentric distances $r \sim 0.3$ –50 AU (e.g., Marsch et al. 1982; Freeman 1988; Gazis et al. 1994; Richardson et al. 1995; Cranmer et al. 2009). Similarly, remote observations taken with the Ultraviolet Coronagraph Spectrometer detect large ion temperatures that increase with heliocentric distance within a few solar radii of the Sun (Kohl et al. 1998; Antonucci et al. 2000). The observed heating likely plays a critical role in accelerating the solar wind to supersonic and super-Alfvénic speeds and also significantly impacts the plasma properties in the near-Earth space environment.

Several heating mechanisms have been proposed to account for these observations, including magnetic reconnection (Fisk 2003; Fisk et al. 2003), plasma instabilities driven by an electron heat flux or cross-field currents (Markovskii & Hollweg 2002a, 2002b; Markovskii 2004), non-turbulent waves at frequencies comparable to the proton cyclotron frequency Ω_i (Abraham-Shrauner & Feldman 1977; Hollweg & Turner 1978; McKenzie et al. 1979; Tu & Marsch 1997; Marsch & Tu 1997; Hollweg & Isenberg 2002), turbulent waves extending from low frequencies up to $\sim \Omega_i$ (Isenberg & Hollweg 1983; Tu et al. 1984; Marsch 1991; Chandran 2005), and turbulence that fluctuates only on timescales $\gg \Omega_i^{-1}$ (Coleman 1968; Matthaeus et al. 1999a; Dmitruk et al. 2001, 2002; Cranmer & van Ballegoijen 2005; Cranmer et al. 2007; Velli et al. 1989; Verdini & Velli 2007; Chandran et al. 2009; Chandran & Hollweg 2009; Verdini et al. 2009). This paper focuses on this last class of models, those involving low-frequency turbulence.

In these models, photospheric motions driven by solar convection launch Alfvén waves that propagate away from the Sun

in the solar-wind frame. Alfvén waves propagating toward the Sun in the solar-wind frame are generated by some combination of non-WKB wave reflection (Heinemann & Olbert 1980; Velli 1993), parametric instabilities (Galeev & Oraevskii 1963; Del Zanna et al. 2001), and velocity-shear instabilities (Roberts et al. 1992). Interactions between oppositely propagating Alfvén waves then cause wave energy to cascade to small scales perpendicular to the magnetic field (λ_{\perp}). However, the correlation lengths of Alfvén wave packets in the direction of the background magnetic field (λ_{\parallel}) remain comparatively long, and the Alfvén-wave frequencies remain $\ll \Omega_i$. When the wave energy cascades to perpendicular scales λ_{\perp} comparable to the proton gyroradius ρ_i , the wave energy begins to dissipate, heating the ambient plasma.

Linear wave theory shows that the properties of low-frequency Alfvénic fluctuations depend strongly upon λ_{\perp} (Hollweg 1999). At $\lambda_{\perp} \gg d_i$, the fluctuations are non-compressive Alfvén waves, where $d_i = v_A/\Omega_i$ is the ion inertial length.⁴ On the other hand, in low- β plasmas at $\rho_i \lesssim \lambda_{\perp} \lesssim d_i$, the fluctuations are highly compressive, in the sense that $\delta n/n_0 > \delta B/B_0$, where δn and n_0 are the fluctuating and background electron densities, and δB and B_0 are the fluctuating and background magnetic fields. For $\beta \sim 1$, $\delta n/n_0 \sim \delta B/B_0$ at $\lambda_{\perp} \sim \rho_i$. At even smaller scales, $\lambda_{\perp} \lesssim \rho_i$, the ion and electron velocities decouple for all β , the waves become dispersive, and the fluctuations produce parallel electric and magnetic field perturbations that cause the waves to damp (Hasegawa & Chen 1976; Quataert 1998; Quataert & Gruzinov 1999; Leamon et al. 1999; Cranmer & van Ballegoijen 2003; Gary & Nishimura 2004). At $\lambda_{\perp} \lesssim \rho_i$, these solutions to the Alfvén-wave branch of the linear dispersion relation are called kinetic Alfvén waves

⁴ For reference, $d_i \simeq \beta^{-1/2} \rho_i$, $\beta = 8\pi p/B^2 \ll 1$ in the corona, and for typical coronal-hole parameters $d_i \sim 3 \times 10^5$ cm at $r \simeq 5 R_{\odot}$; by contrast, $\beta \sim 0.2$ –1 in the near-Earth solar wind at ~ 1 AU and $d_i \sim 3 \times 10^6$ cm.

(KAWs). Many of the measured properties of the magnetic and electric field fluctuations in the near-Earth solar wind are consistent with KAW turbulence on small scales (e.g., Howes et al. 2008a, 2008b; Sahraoui et al. 2009, and references therein).

The goal of this paper is to test the importance of low-frequency turbulence in the solar wind using measurements of density fluctuations. Coles & Harmon (1989) measured the spectrum of electron density fluctuations in the corona at radii as small as $5 R_{\odot}$. In addition, measurements of density fluctuations in the solar wind at ~ 1 AU have been carried out using a variety of methods (e.g., Celnikier et al. 1983, 1987; Hnat et al. 2005; Kellogg & Horbury 2005). Because oblique Alfvén waves become increasingly compressive as λ_{\perp} decreases to values $\lesssim d_i$, the observed density fluctuation spectrum constrains the spectrum of oblique Alfvén waves and provides an upper limit on the heating rate ϵ from Alfvénic turbulence. In Section 2, we summarize the predicted density fluctuations induced by low-frequency Alfvénic turbulence and describe some of the remaining uncertainties in these predictions (see also Schekochihin et al. 2009). We then show how the measured density fluctuations in coronal holes and at ~ 1 AU constrain the turbulent heating rate (Section 3). In Section 4, we describe the “sweeping” model for coronal heating, in which the corona is heated by cyclotron damping of kHz-range waves launched directly from the Sun; we present a simple explanation for why radio observations do not rule out turbulent heating models, even though they appear to rule out the sweeping model (as was shown by Hollweg 2000). In Section 5, we summarize and discuss our results. Our analysis and results are broadly similar to those of Harmon & Coles (2005), but we consider a different model for the turbulent cascade of Alfvén waves, and apply the density fluctuation constraint both to remote observations of turbulence in coronal holes and to in situ measurements of turbulence in the near-Earth solar wind.

2. PREDICTED DENSITY FLUCTUATIONS IN LOW-FREQUENCY ALFVÉNIC TURBULENCE MODELS

In this section, we briefly summarize the density fluctuations produced by low-frequency Alfvénic turbulence (see Lithwick & Goldreich 2001 and Schekochihin et al. 2009 for a more comprehensive discussion). We assume that the Alfvén wave power spectrum follows the “critical balance” theory of Goldreich & Sridhar (1995). In doing so, we implicitly assume that the turbulence is “balanced,” i.e., that there are equal fluxes of Alfvén waves propagating toward and away from the Sun in the plasma frame, or equivalently, that there is zero cross helicity; we discuss the effects of a non-zero cross helicity at the end of the section.

Although Alfvén waves themselves are not compressive when $k_{\perp} d_i \ll 1$ (where k_{\perp} and k_{\parallel} are the components of the wave vector \mathbf{k} perpendicular and parallel to the background magnetic field), low-frequency Alfvénic turbulence nonetheless produces significant density fluctuations via two different physical processes. First, as energy cascades to scales $\lesssim d_i$, Alfvén waves transition to KAWs, which are compressive (see Figure 3 discussed below). Second, both slow waves and entropy modes are passively mixed by the Alfvénic cascade (Lithwick & Goldreich 2001). Because the Alfvénic fluctuations have an anisotropic Kolmogorov spectrum, the density fluctuations associated with the entropy modes and/or slow waves also have an anisotropic Kolmogorov spectrum (Maron & Goldreich 2001).

For the collisionless conditions appropriate to the solar corona and solar wind, the entropy modes and slow waves are both

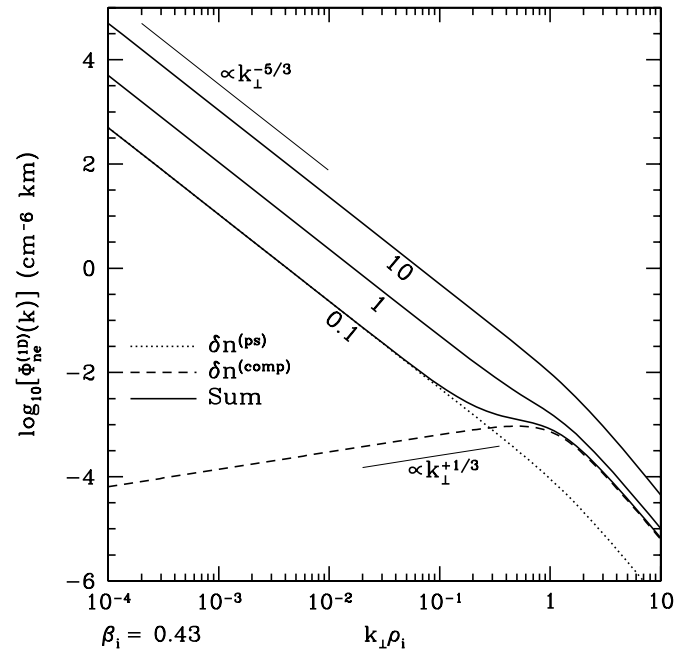


Figure 1. One-dimensional density fluctuation power spectrum $\Phi_{ne}^{(1D)}$ produced by balanced low-frequency Alfvénic turbulence in the near-Earth solar wind with $\beta_i = 0.43$ and $T_i/T_e = 1$. Total density fluctuation spectra (solid) are shown for $f = 0.1, 1$, and 10 , with the separate passive-scalar component (dotted) and “active” KAW component (dashed) shown explicitly for $f = 0.1$.

damped, but their damping rates are $\sim k_{\parallel} v_{th,p}$, where $v_{th,p}$ is the proton thermal speed.⁵ The cascade rate is $\sim k_{\perp} \delta v_k \sim k_{\parallel} v_A$, where δv_k is the rms amplitude of the velocity fluctuation at a perpendicular scale k^{-1} (where $k \simeq k_{\perp}$ since $k_{\perp} \gg k_{\parallel}$). The cascade rate is thus comparable to the linear Alfvén wave frequency. For $\beta \lesssim 1$, the slow waves and entropy modes cascade faster than they are damped, and the passive scalar contribution to the density fluctuations extends to small scales $\sim \rho_i$ (Lithwick & Goldreich 2001). (We discuss the case of $\beta \gtrsim 1$ later in this section.)

Figure 1 summarizes our prediction for the one-dimensional density fluctuation spectrum $\Phi_{ne}^{(1D)}$ associated with balanced (zero cross-helicity) low-frequency Alfvénic turbulence. The density fluctuations associated with the slow waves and entropy modes are cascaded by the Alfvénic fluctuations like a passive scalar and, at perpendicular scale k^{-1} , their rms value is denoted by $\delta n_k^{(ps)}$. The rms density fluctuations that arise from the KAW compressions are denoted by $\delta n_k^{(comp)}$. At large scales, the passive-scalar density fluctuation spectrum is chosen to be proportional to the perpendicular kinetic energy spectrum⁶ associated with the perpendicular velocity fluctuation $\delta v_{\perp k}$. The latter is determined using the analytic cascade model of Howes et al. (2008a), which is based on the assumptions of local nonlinear energy transfer in wavenumber space together with the critical balance between linear propagation and nonlinear interaction times. The analytic model smoothly transitions from anisotropic Kolmogorov Alfvén-wave turbulence at $k_{\perp} \rho_i \ll 1$ to anisotropic KAW turbulence at $k_{\perp} \rho_i \gg 1$; it agrees well

⁵ Under these conditions, there are really two entropy modes, one associated with the electrons and the other associated with the protons. The former is strongly damped, at a rate $\sim k v_{th,e}$, while the latter is less strongly damped. We focus on the latter throughout.

⁶ For small scales $k_{\perp} \rho_i \gtrsim 1$, the passive-scalar density spectrum follows perpendicular magnetic energy spectrum rather than the perpendicular kinetic energy spectrum.

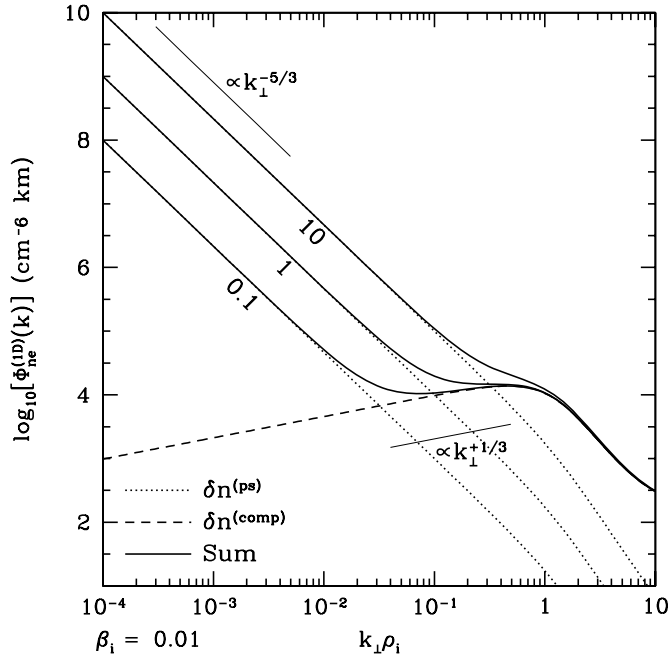


Figure 2. One-dimensional density fluctuation power spectrum $\Phi_{nc}^{(1D)}$ produced by low-frequency Alfvénic turbulence in coronal holes with $\beta_i = 0.01$ and $T_i/T_e = 2$. Total density fluctuation spectra (solid) are shown for $f = 0.1, 1$, and 10 , with the separate passive-scalar component (dotted) and “active” KAW component (dashed) shown explicitly for each case.

with numerical simulations of kinetic turbulence in the (limited) comparisons available to date (Howes et al. 2008b). The value of $\delta n_k^{(comp)}$ in Figure 1 is determined from the value of $\delta v_{\perp k}$ in the analytic cascade model by assuming that $\delta n_k^{(comp)}/\delta v_{\perp k}$ equals the ratio of the density fluctuation to the velocity fluctuation in a linear KAW at the same wave vector in linear Vlasov theory (Stix 1992).

The relative magnitude of the passive and active density fluctuations is uncertain and may vary with position (and time) in the solar wind. We determine the constant of proportionality between the passive-scalar density spectrum and the kinetic energy spectrum by specifying the ratio

$$f \equiv \left[\frac{\delta n_k^{(ps)}/n_0}{\delta v_{\perp k}/v_A} \right]_{k=k_0}^2, \quad (1)$$

where $2\pi/k_0$ is the driving scale or outer scale of the turbulence. Figure 1 presents one-dimensional density spectra from solutions of the cascade model for near-Earth solar-wind conditions. Plasma parameters for this figure have been chosen to correspond to period II of Celnikier et al. (1987): $B_0 = 1.5 \times 10^{-4}$ G, $n_i = 18 \text{ cm}^{-3}$, $T_i = T_e = 1.54 \times 10^5$ K, and $v_{sw} = 460 \text{ km s}^{-1}$, giving $\rho_i = 2 \times 10^6$ cm. We assume a driving scale $2\pi/k_0 = 2 \times 10^{11}$ cm, giving cascade model parameters $\beta_i = 8\pi n k_B T_i/B_0^2 = 0.43$, $T_i/T_e = 1$, and $k_0\rho_i = 6 \times 10^{-5}$.

Figure 1 shows the total density fluctuation spectra (solid) for $f = 0.1, 1$, and 10 , with the separate passive-scalar component (dotted) and “active” KAW component (dashed) shown explicitly for the $f = 0.1$ case. The $f = 0.1$ case demonstrates that the passively mixed density fluctuations have a Kolmogorov power-law spectrum at large scales (small k) with a break at $k_{\perp}\rho_i \sim 1$ where the turbulence transitions to dispersive KAWs. On small scales, however, the “active” density fluctuations due to KAWs become important and can

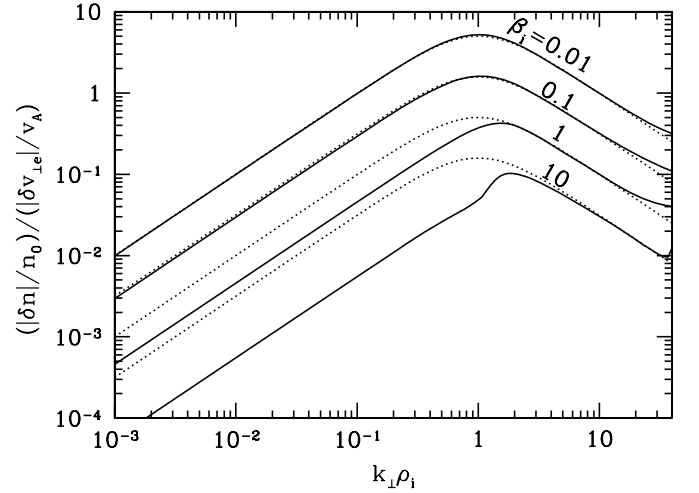


Figure 3. Density fluctuations relative to the perpendicular electron velocity fluctuations $(\delta n_k/n_0)/(\delta v_{\perp ke}/v_A)$ for $\beta_i = 0.01, 0.1, 1$, and 10 , (solid) based on linear Vlasov–Maxwell theory for KAWs. Dotted lines are the predictions given by Equation (2) with $\gamma_i = 1$.

dominate over the passive contribution. The density fluctuation spectrum associated with the KAWs is a factor of $\sim k_{\perp}^2$ flatter than Kolmogorov for $k_{\perp}\rho_i \lesssim 1$. Indeed, the one-dimensional density-fluctuation spectrum from KAW compressions is rising, $\propto k_{\perp}^{1/3}$, for $k_{\perp}\rho_i \lesssim 1$. This is because the density perturbation due to a linear KAW is $\propto k_{\perp}$ times the velocity perturbation in this limit (see Equation (2) below).

The $f = 0.1$ result in Figure 1 may be compared directly⁷ to the measured density spectrum for this period of solar-wind turbulence shown in Figure 5 of Celnikier et al. (1987). The predicted density spectrum, combining both a passive-scalar contribution and compressive KAWs, qualitatively reproduces the measured spectrum. Note that the assumption of balanced turbulence (zero cross helicity) is not an unreasonable assumption for this interval of relatively slow solar wind. In addition, the value $f = 0.1$ is consistent with several observations that are discussed following Equation (3) below.

In coronal holes, where $\beta_i \ll 1$, the compressive motions associated with the KAWs become comparatively stronger. Figure 2 presents cascade-model results analogous to Figure 1 for parameters appropriate to coronal holes: $\beta_i = 0.01$, $T_i/T_e = 2$, and $k_0\rho_i = 10^{-8}$.⁸ The absolute normalization of the density fluctuations was chosen to roughly match the observations of Coles & Harmon (1989) in coronal holes. Total density fluctuation spectra (solid) are shown for $f = 0.1, 1$, and 10 , with the decomposition into passive-scalar component (dotted) and “active” KAW component (dashed) included for each case. The results in Figure 2 are similar to those in Figure 1 except that the active KAW component of the density fluctuations is more prominent at low β_i . The questionable assumption of balanced (zero cross-helicity) turbulence in coronal holes is discussed in detail at the end of this section.

Figure 3 focuses on the density fluctuations due to linear KAWs, showing results as a function $k_{\perp}\rho_i$ for several β_i . For $\beta \lesssim 1$, the relation between the density and velocity fluctuations

⁷ Note that a value of $k_{\perp}\rho_i = 1$ in Figure 1 corresponds to a frequency of 3.6 Hz in Figure 5 of Celnikier et al. (1987).

⁸ In the cascade model, k_0 is not the actual outer-scale wavenumber. Instead, in the case of the corona, it is the much smaller wavenumber at which the anisotropic power spectrum would extrapolate to isotropic fluctuations with $\delta B = B_0$ (Howes et al. 2008a).

of a KAW at wavevector \mathbf{k} , denoted by δn_k and $\delta v_{\perp k}$, can be derived analytically using a two-fluid model and is given by (Hollweg 1999, Equation (51))

$$\left| \frac{\delta n_k}{n_0} \right| = \frac{k_{\perp} d_i}{(1 + \gamma_i k_{\perp}^2 \rho_i^2)} \left| \frac{\delta v_{\perp k}}{v_A} \right|, \quad (2)$$

assuming that $k_{\perp} \gg |k_{\parallel}|$ and $\omega \ll \Omega_i$, where ω is the wave frequency and γ_i is the adiabatic index of the ions. In addition to showing the (normalized) ratio of density fluctuations to velocity fluctuations from linear kinetic theory (solid), Figure 3 also shows the values predicted by Equation (2) (dotted) with $\gamma_i = 1$. This figure demonstrates that the density fluctuations are reduced by a factor of $\sim \beta$ when $\beta \gtrsim 1$ as expected, because the fluctuations become increasingly incompressible for high β . An additional change in the predicted density fluctuations for $\beta \gtrsim 1$ —as can occur in the solar wind at ~ 1 AU—is that the damping time of slow waves and entropy modes becomes shorter than their expected cascade times. Because the solar wind is collisionless, this occurs even on large scales. As a result, the passive contribution to the density fluctuations may be significantly diminished when $\beta \gtrsim 1$ (Lithwick & Goldreich 2001).

Equation (2) can be used to estimate the ratio between the passive-scalar density fluctuation and the density fluctuation arising from KAW compressions. We assume that $\delta n_k^{(\text{comp})}/\delta v_{\perp k}$ equals the ratio $\delta n_k/\delta v_{\perp k}$ for linear KAWs given by Equation (2). When $\beta \lesssim 1$ and the cross helicity is zero, $\delta n_k^{(\text{ps})}/\delta v_{\perp k}$ is independent of k within the inertial range. Assuming that $\delta n_k^{(\text{ps})}/\delta v_{\perp k}$ remains roughly constant from the outer scale all the way to $k_{\perp} \sim \rho_i^{-1}$, Equation (2) implies that for balanced turbulence with $\beta \lesssim 1$

$$\left[\frac{\delta n_k^{(\text{comp})}}{\delta n_k^{(\text{ps})}} \right]_{k=\rho_i^{-1}} \sim (\beta f)^{-1/2}. \quad (3)$$

At 1 AU, the value of $\delta n_k^{(\text{ps})}/n_0$ at $k = k_0$ ranges from roughly 0.1 to 0.3, as the assumed outer-scale timescale (as measured in the spacecraft frame) of the turbulence is varied from 1–12 hr (Tu & Marsch 1995, Figure 2-14). If we set $v_A = 77 \text{ km s}^{-1}$ as in Celnikier’s period II data and $\delta v_{\perp k} \simeq 30 \text{ km s}^{-1}$ at $k = k_0$ at 1 AU (see Cranmer & van Ballegoijen 2005, Figure 9), then $f \simeq 0.07\text{--}0.6$. Equation (3) thus suggests that KAW compressions usually dominate the density fluctuations on small scales ($k_{\perp} \rho_i \sim 1$) at 1 AU.

It is important to note several theoretical uncertainties in our predictions for the density fluctuations that should accompany low-frequency Alfvénic turbulence in the solar wind. First, the relative amplitudes of the slow waves, entropy modes, and Alfvén waves on large scales are not precisely known. Therefore, we present several values of f in Figures 1 and 2. A second, and more significant, limitation is that we have assumed that the turbulence is “balanced” (zero cross-helicity), i.e., that the energy in waves propagating toward the Sun (in the solar-wind frame) equals the energy in waves propagating away from the Sun. This is generally not observed to be true at ~ 1 AU (particularly in the fast wind; Grappin et al. 1990; Tu & Marsch 1990). Closer to the Sun there is an even larger difference between the energies of Sunward and anti-Sunward waves (Roberts et al. 1987; Bavassano et al. 2000). Non-zero cross helicity or “imbalance” affects strong Alfvénic turbulence in several ways. For example, nonlinear interactions

among Alfvén waves occur only between waves propagating in opposite directions in the plasma frame (Iroshnikov 1963; Kraichnan 1965), and so if the energy in waves propagating toward the Sun is very small, then the energy cascade rate and turbulent heating rate also become small (Dobrowolny et al. 1980; Hossain et al. 1995; Chandran et al. 2009). Finite cross helicity may also modify the wavenumber scalings of the inertial-range power spectra of the density, magnetic field, and velocity. Because the “minority” Sunward Alfvén waves and the passive scalar fluctuations are both cascaded by the “dominant” anti-Sunward Alfvén waves, the passive scalar spectrum is expected to have the same inertial-range scaling as the Sunward waves (Lithwick & Goldreich 2003; Chandran 2008b). In some studies of Alfvénic turbulence with cross helicity (e.g., Grappin et al. 1983; Chandran 2008a; Beresnyak & Lazarian 2009) the minority Alfvén waves have a shallower power spectrum than the dominant Alfvén waves, suggesting that the passive scalar spectrum is shallower than the magnetic spectrum in highly imbalanced turbulence. This finding may be related to the shallow density spectra seen in radio observations of the corona, in which the turbulence is expected to be highly “imbalanced” (Cranmer & van Ballegoijen 2005; Verdini & Velli 2007).⁹ However, a number of other studies find that the inertial-range spectra of the minority waves and dominant waves scale with wavenumber in the same way (Lithwick et al. 2007; Perez & Boldyrev 2009; Podesta & Bhattacharjee 2009). Moreover, the different studies cited above disagree over whether the spectra of the minority and dominant waves are equal at the dissipation scale (“pinning”). Because imbalanced Alfvénic turbulence is still not fully understood, and is likely the norm in the solar wind, we are only able to derive upper limits on the turbulent heating rates from the density observations, as discussed further below. In addition, this uncertainly implies that the precise power-law scalings for $\Phi_{\text{ne}}^{\text{ID}}$ in Figures 1 and 2 should not be taken too literally, although we believe that our conclusions about the relative contribution of the active and passive density fluctuations are robust.

3. OBSERVATIONAL CONSTRAINTS ON LOW-FREQUENCY ALFVÉNIC TURBULENCE MODELS

In this section, we discuss observational constraints on density fluctuations in the solar corona and solar wind, and their implications for low-frequency Alfvénic turbulence models.

3.1. Coronal Holes

Coles & Harmon (1989) analyzed the spectral broadening of Arecibo radar observations of Venus near superior conjunction to determine the three-dimensional power spectrum of electron density fluctuations $\Phi_{\text{ne}}(r, k)$ (treated as an isotropic function of wave vector \mathbf{k}) at a range of heliocentric distances r in the slow solar wind. They were able to fit $\Phi_{\text{ne}}(r, k)$ at $r = 5 R_{\odot}$ with one power law at $k < 10^{-7} \text{ cm}^{-1}$, a slightly shallower power law at $10^{-7} \text{ cm}^{-1} < k < k_i$, and an exponential or Gaussian at $k > k_i$, where

$$k_i \simeq 10^{-5} \text{ cm}^{-1} \quad (4)$$

⁹ For example, Markovskii & Hollweg (2002a, 2002b) fit the one-dimensional density spectrum at $r = 5 R_{\odot}$ and at $k < 10^{-7} \text{ cm}^{-1}$ with a power law of the form $k^{-1.2}$ and a power law of the form $k^{-2/3}$ at $10^{-7} \text{ cm}^{-1} < k < 10^{-5} \text{ cm}^{-1}$. The density fluctuations at $k < 10^{-7} \text{ cm}^{-1}$ in their study are thought to correspond to inertial-range passive-scalar fluctuations.

is the “inner-scale” wavenumber at $r = 5 R_\odot$. They found that at $k = k_i$ and $r = 5 R_\odot$, $\Phi_{ne} \simeq 9.0 \times 10^3 \text{ cm}^{-6} \text{ km}^3$ (see their Figure 4). We focus on the inner scale for reasons that will become clearer below. Coles et al. (1995) found that Φ_{ne} is a factor of $\simeq 15$ smaller in coronal holes than in the slow wind, and thus we set

$$\Phi_{ne}(r = 5 R_\odot, k = 10^{-5} \text{ cm}^{-1}) \simeq 6.0 \times 10^2 \text{ cm}^{-6} \text{ km}^3. \quad (5)$$

The rms electron density fluctuation δn_{k_i} is given by $\delta n_{k_i}^2 \simeq 4\pi k_i^3 \Phi_{ne}(k_i)$, which implies $\delta n_{k_i} \simeq 87 \text{ cm}^{-3}$ at $r = 5 R_\odot$. We estimate the coronal-hole electron density from Equation (4) of Feldman et al. (1997), which gives $n_e = 5.9 \times 10^3 \text{ cm}^{-3}$ at $r = 5 R_\odot$; this is very close to the value inferred by Fisher & Guhathakurta (1995) from observations taken with the *Spartan* 201-01 coronagraph. This value for the background density then gives

$$\frac{\delta n_{k_i}}{n_0} \simeq 1.5 \times 10^{-2} \quad (6)$$

at $r = 5 R_\odot$.

An upper limit on the rms amplitude of the Alfvénic velocity fluctuation at perpendicular scale k_i^{-1} , denoted δv_{k_i} , can be obtained by assuming that the density fluctuations at scale k_i^{-1} arise entirely from KAWs. Using the linear eigenfunctions of KAWs, we can write

$$\frac{\delta v_{k_i}}{v_A} \lesssim \left(\frac{1 + \gamma_i k_i^2 \rho_i^2}{k_i d_i} \right) \frac{\delta n_{k_i}}{n_0}. \quad (7)$$

If the compressibility of the KAWs noticeably affects the density spectrum from $10^{-7} \text{ cm}^{-1} < k < 10^{-5} \text{ cm}^{-1}$, as conjectured above and as is suggested by Figure 2, then δv_{k_i} may be close to the upper limit given in Equation (7); this is because the fraction of Φ_{ne} that arises from KAWs increases at larger k (Figure 2). To evaluate the right-hand side of Equation (7) we assume $\gamma_i = 1$ and $T_i = 2.0 \times 10^6 \text{ K}$ and adopt the coronal-hole magnetic field model of Cranmer & van Ballegoijen (2005, their Equation (2)), which gives $B_0 = 5.8 \times 10^{-2} \text{ G}$ at $r = 5 R_\odot$. These parameters give $\rho_i = 2.3 \times 10^4 \text{ cm}$, $d_i = 3 \times 10^5 \text{ cm}$, $v_A = 1.6 \times 10^8 \text{ cm s}^{-1}$, and

$$\frac{\delta v_{k_i}}{v_A} \lesssim 0.35 \left(\frac{\delta n_{k_i}}{n_0} \right), \quad (8)$$

or, equivalently,

$$\delta v_{k_i} \lesssim 8.4 \text{ km s}^{-1}. \quad (9)$$

At $k = k_i$, the density spectrum at $r = 5 R_\odot$ is still close to the value obtained by extrapolating a power-law fit to Φ_{ne} for values of k between 10^{-7} cm^{-1} and 10^{-6} cm^{-1} . We can thus assume that most of the cascade power is still present at $k_\perp = k_i$ and that most of the dissipation occurs at $k_\perp > k_i$. Moreover, because $k_i \rho_i \simeq 0.2$, the kinetic energy and magnetic energy of Alfvénic fluctuations at $k_\perp = k_i$ are comparable, as in incompressible MHD, but not like the short-wavelength regime $k_\perp \rho_i \gg 1$, in which the magnetic energy dominates. The energy density of Alfvénic fluctuations at scale k_i^{-1} is thus $\simeq \rho \delta v_{k_i}^2$. The time required for the fluctuation energy at $k_\perp = k_i$ to cascade to $k_\perp \geq 2k_i$, denoted by t_c , satisfies the inequality

$$t_c \gtrsim (k_i \delta v_{k_i})^{-1}. \quad (10)$$

The right-hand side of Equation (10) is the shearing timescale for an Alfvénic velocity fluctuation at $k_\perp = k_i$ with rms amplitude δv_{k_i} . This is a lower-limit on t_c because in incompressible MHD, the anti-Sunward waves are sheared by waves propagating toward the Sun (Iroshnikov 1963; Kraichnan 1965), as summarized in Section 2. Thus, if the Sunward waves are much less energetic than the anti-Sunward waves at $k_\perp = k_i$, the time required for Sunward waves to shear and substantially distort anti-Sunward waves is much greater than $(k_i \delta v_{k_i})^{-1}$ (Lithwick et al. 2007; Beresnyak & Lazarian 2008; Chandran 2008a). The cascade power in low-frequency Alfvén-wave turbulence at $r = 5 R_\odot$, denoted by ϵ , is roughly $\rho v_{k_i}^2 / t_c$. Given Equation (10), we can write

$$\epsilon \lesssim c_0 \rho k_i \delta v_{k_i}^3, \quad (11)$$

where c_0 is a dimensionless constant that is chosen by equating the right-hand side of Equation (11) with the cascade power in strong Alfvén-wave turbulence with equal fluxes of Alfvén waves propagating parallel and anti-parallel to the background magnetic field. The value of c_0 is not precisely known; here we follow Howes et al. (2008a) in setting $c_0 = 0.25$. Substituting Equation (9) into Equation (11), we find

$$\epsilon \lesssim 1.5 \times 10^{-8} \text{ erg cm}^{-3} \text{ s}^{-1}. \quad (12)$$

This upper limit can be compared with the parameterized heating rates employed in empirical models of the fast solar wind. Allen et al. (1998) constructed a series of two-fluid models with heating rates chosen to match in situ measurements of the fast wind at 1 AU as well as the coronal-hole density profile inferred from the brightness profile of electron-scattered, polarized white light (Fisher & Guhathakurta 1995). In these models, denoted by SW2, SW3, and SW4, the total (electron plus proton) heating rates at $r = 5 R_\odot$ were $3.1 \times 10^{-9} \text{ erg cm}^{-3} \text{ s}^{-1}$, $1.4 \times 10^{-8} \text{ erg cm}^{-3} \text{ s}^{-1}$, and $6.8 \times 10^{-9} \text{ erg cm}^{-3} \text{ s}^{-1}$, respectively. Esser et al. (1997) constructed similar models with higher temperatures at the coronal base and lower heating rates. The value of ϵ at $r = 5 R_\odot$ was $2 \times 10^{-10} \text{ erg cm}^{-3} \text{ s}^{-1}$ in their model A and $8 \times 10^{-10} \text{ erg cm}^{-3} \text{ s}^{-1}$ in their model B.¹⁰ Since these models (by construction) provide a reasonable fit to the observed properties of the fast wind, we take the actual heating rate in coronal holes at $r = 5 R_\odot$ to be in the range spanned by these models, i.e., between $2 \times 10^{-10} \text{ erg cm}^{-3} \text{ s}^{-1}$ and $1.4 \times 10^{-8} \text{ erg cm}^{-3} \text{ s}^{-1}$. Since the upper limit in Equation (12) is above this range, we conclude that a model in which the fast wind is accelerated by heating from low-frequency Alfvénic turbulence is consistent with the radio observations. Future investigations could provide tighter constraints on the fraction of δn_{k_i} that arises directly from KAWs as well as the ratio of Sunward to anti-Sunward wave energy at $k_\perp = k_i$, which could in principle lower the upper limit on ϵ that is implied by the density fluctuation measurements.

3.2. The Solar Wind at $\sim 1 \text{ AU}$

Measurements of density fluctuations in the solar wind at $\sim 1 \text{ AU}$ have been carried out using a variety of methods (e.g., Celnikier et al. 1983, 1987; Hnat et al. 2005; Kellogg & Horbury 2005); these allow us to calculate an upper limit on the heating

¹⁰ For comparison, the heating rate at $r = 5 R_\odot$ was $3 \times 10^{-10} \text{ erg cm}^{-3} \text{ s}^{-1}$ in the theoretical model of Markovskii & Hollweg (2002a, 2002b), and between $8 \times 10^{-10} \text{ erg cm}^{-3} \text{ s}^{-1}$ and $5 \times 10^{-9} \text{ erg cm}^{-3} \text{ s}^{-1}$ in the “sweeping” models of Marsch & Tu (1997).

by low-frequency Alfvénic turbulence analogous to that derived in the previous section.

For concreteness, we use Celnikier et al.'s (1987) period II to find an upper limit to the KAW contribution to the density fluctuations, but similar results are obtained from other measurements. From their Figure 7, we infer that $\delta n_k/n_0 \lesssim 10^{-2}$ at $k_{\perp}\rho_i \simeq 0.3$,¹¹ where $B \simeq 1.5 \times 10^{-4}$ G, $n_0 \simeq 18 \text{ cm}^{-3}$, $T_p \simeq 1.5 \times 10^5$ K, $\rho_p \simeq 2 \times 10^6$ cm, $v_A \simeq 77 \text{ km s}^{-1}$, $v_{\text{wind}} \simeq 460 \text{ km s}^{-1}$, and $\beta \simeq 0.43$ in this epoch of data. Unlike in the observations of the solar corona described in Section 3.1, there is no clear evidence for an inner scale to the density fluctuations at 1 AU. Given the lack of a preferred scale, we evaluate the density fluctuations at $k_{\perp}\rho_i \simeq 0.3$ as a compromise between the scales where the KAW density fluctuations peak ($k_{\perp}\rho_i \sim 1$) and the scales where incompressible MHD is a reasonable model for the cascade ($k_{\perp}\rho_i \ll 1$); our conclusions are, however, insensitive to reasonable variations about this choice.

A limit on the density fluctuations due to KAWs of $\delta n_k/n_0 \lesssim 10^{-2}$ at $k_{\perp}\rho_i \simeq 0.3$ corresponds to a limit on the velocity fluctuations of $\delta v_k/v_A \lesssim 10^{-2}$ at the same scale (i.e., $\delta v_k \lesssim 1 \text{ km s}^{-1}$) and thus to a limit on the heating rate due to low-frequency Alfvénic turbulence of

$$\epsilon \lesssim 5 \times 10^{-16} \text{ erg cm}^{-3} \text{ s}^{-1}. \quad (13)$$

At ~ 1 AU, the heating rate in the solar wind can be directly measured from the non-adiabatic temperature profile of the protons and electrons, using $\epsilon \simeq \rho v_r T ds/dr$. For example, using the proton data from Voyager 2 (e.g., Matthaeus et al. 1999b), we infer that $\epsilon \simeq 3 \times 10^{-16} \text{ erg cm}^{-3} \text{ s}^{-1}$ is required to explain the non-adiabaticity of the solar wind at 1 AU.¹² The close correspondence between this measured heating rate at 1 AU and the upper limit in Equation (13) implies that, if low-frequency Alfvénic turbulence contributes to heating the solar wind at ~ 1 AU, direct density fluctuations due to compressive KAWs must contribute significantly to the measured density fluctuations at $k_{\perp}\rho_i \sim 1$. In this context, we note that Kellogg & Horbury (2005) have argued for an ion-acoustic or KAW origin for the small-scale density fluctuations in the solar wind at 1 AU using completely independent arguments. It is also important to note that the Celnikier et al. measurements are in the relatively slow solar wind ($v \simeq 450 \text{ km s}^{-1}$), in which the turbulence is observed to be fairly balanced (Grappin et al. 1990). Thus, the cascade time is likely comparable to the lower limit in Equation (10), in which case the cascade power can also be comparable to the upper limit in Equation (13).

The density fluctuation measurements of Celnikier et al. (1987) show a break from a Kolmogorov spectrum at low k to a flatter spectrum at high k . This is qualitatively consistent with the expectations from Figure 1. The observed break happens at a rest frame frequency of $\simeq 0.1$ Hz (Celnikier et al. 1987), which corresponds to $k^{-1} \simeq 7 \times 10^7 \text{ cm} \gg \rho_i$, $d_i \sim 3 \times 10^6 \text{ cm}$ using the Taylor hypothesis. This suggests that $f \ll 1$, i.e., that the passive scalar contribution to the density fluctuations is small compared to the KAW contribution, so that the latter begins to

dominate at $k_{\perp}\rho_i \ll 1$ (see Figure 1). A small value of f at 1 AU is not implausible given the observations described above, following Equation (3).

4. OBSERVATIONAL CONSTRAINTS ON THE “SWEEPING” MODEL OF CYCLOTRON HEATING

An alternative mechanism for heating coronal holes is ion-cyclotron heating by non-turbulent high-frequency (kHz-range) waves. One of the proposed sources for these kHz-range waves is magnetic reconnection in the photosphere or chromosphere (Axford & McKenzie 1992). Because B_0 and Ω_i decrease with increasing r , waves with $\omega < \Omega_i$ at the base of the corona eventually reach radii at which $\omega \simeq \Omega_i$, at which point the waves undergo cyclotron damping and heat the ions. If a broad frequency spectrum of waves is launched from the Sun, the waves will result in radially extended ion heating, with lower-frequency waves causing heating farther from the Sun (Schwartz et al. 1981; Axford & McKenzie 1992; Marsch & Tu 1997; Tu & Marsch 1997; Ruzmaikin & Berger 1998; Czechowski et al. 1998). Although cyclotron heating could in principle explain the observed temperature anisotropies of ions in the corona and fast solar wind, this “sweeping” or “direct-launching” model faces a significant difficulty. If the waves are oblique, with wave vectors that make a nonzero angle θ with respect to \mathbf{B}_0 , then the waves induce density fluctuations at high frequencies. Hollweg (2000) investigated this effect, modeling the wave obliquity by setting $\theta = 60^\circ$. Using the wave power spectra employed in the “sweeping” models of Marsch & Tu (1997), he found that the waves would induce larger density fluctuations than are detected by radio observations, by a factor of $>10^2$ at $k = 0.3 \times 10^{-5} \text{ cm}^{-1}$. Tu & Marsch (2001a, 2001b) have responded to this criticism by suggesting that transit-time damping could remove the obliquely propagating waves and thereby reduce the density fluctuations. We believe, however, that “phase mixing” by laminar (Heyvaerts & Priest 1983) and turbulent (Chandran 2008b) density structures will transfer Alfvén-wave energy to larger k_{\perp} , thereby significantly limiting the amount of Alfvén/ion-cyclotron wave energy that can remain at small θ as the waves propagate from the coronal base out to $r = 5 R_{\odot}$.

4.1. Why Radio Observations Rule Out the “Sweeping” Model but not Turbulent Heating

In the “sweeping” or “direct-launching” model, the heating rate from high-frequency waves Q_{hf} satisfies

$$Q_{\text{hf}} \sim \frac{\mathcal{E}_{\text{hf}}}{t_{\text{pr}}}, \quad (14)$$

where \mathcal{E}_{hf} is the energy density of waves with frequencies between $0.5\Omega_i$ and Ω_i and t_{pr} is the time for Alfvén waves to propagate through the distance over which the magnetic field strength decreases by a factor of 2. Neglecting the solar-wind bulk-flow speed, and assuming $B_0 \propto r^{-2}$, the value of t_{pr} is $\sim 0.4r/v_A$, which is $\simeq 800$ s at $r = 5 R_{\odot}$ in our model coronal hole. On the other hand, in the turbulent-heating model, the heating rate for low-frequency turbulence Q_{lf} satisfies

$$Q_{\text{lf}} \sim \frac{\mathcal{E}_{\text{lf}}}{t_c}, \quad (15)$$

where \mathcal{E}_{lf} is the energy density of low-frequency Alfvénic fluctuations with $0.5k_i < k_{\perp} < k_i$, and t_c is the cascade time at

¹¹ This corresponds to a satellite-frame frequency $\simeq 1$ Hz.

¹² Cranmer & Van Ballegoijen (2005) and Cranmer et al. (2009) find similar heating rates at 1 AU. Celnikier et al. (1987) do not report the electron temperature for their solar-wind epochs, but the mean electron temperature for this solar-wind speed is $\simeq 1.5 \times 10^5$ K (Newbury et al. 1998), which is comparable to T_p . We thus expect the electron heating rate to be at most comparable to the proton heating rate; the proton heating rate is thus a reasonable proxy for the total heating rate, at the factor of 2 level.

$k_{\perp} = k_i$. Equations (9) and (10) imply $t_c \gtrsim 0.1$ s, so that t_c may be as much as 4 orders of magnitude smaller than t_{pr} . For a fixed heating rate and $t_c \ll t_{pr}$, the turbulent-heating model requires much less fluctuation energy at small scales than the sweeping model. In addition, because the compressibility of anisotropic KAWs is comparable to that of oblique ion-cyclotron waves, the turbulent-heating model also requires much lower density fluctuations than the sweeping model for a fixed heating rate when $t_c \ll t_{pr}$.

5. CONCLUSION

In this paper, we have used density fluctuation measurements to test models in which the solar wind is heated by low-frequency Alfvén-wave turbulence; the turbulent fluctuations are assumed to satisfy the inequality $k_{\perp} \gg |k_{\parallel}|$. The density fluctuation measurements—many of which are based on scintillation at radio wavelengths—place an upper limit on the amplitude of oblique Alfvén waves at small scales, where the waves become compressive and induce density fluctuations. This upper limit in turn implies an upper limit on the turbulent heating rate contributed by low-frequency Alfvén-wave turbulence. We calculate this upper limit for coronal holes at $r = 5 R_{\odot}$ and the near-Earth solar wind at 1 AU. The upper limit on the turbulent heating rate we derive (Equation (11)) can be realized only if two conditions are satisfied: (1) most of the measured small-scale density fluctuations are in fact from Alfvén-wave/KAW compressions, and (2) the energy cascade time is $\simeq (k_{\perp} \delta v_{k_{\perp}})^{-1}$ at small scales. The latter is only expected to be the case if there is comparable energy in Sunward and anti-Sunward waves at small scales (where the wave-propagation direction is specified in the solar-wind frame). However, it is currently unclear whether the Sunward and anti-Sunward wave fluxes are equal at small scales (especially in coronal holes), which is one of the primary reasons that density fluctuations can only place an upper limit on the heating rate produced by low-frequency Alfvénic turbulence. (In their related analysis Harmon & Coles (2005) implicitly assumed that the turbulence is balanced.)

The upper limit on the turbulent heating rate at $r = 5 R_{\odot}$ in coronal holes exceeds the parameterized turbulent heating rates employed in models of the fast solar wind, by a factor of a few to ~ 100 depending on the models (Section 3.1). At 1 AU, on the other hand, the upper limit on the turbulent heating rate due to low-frequency Alfvénic turbulence is within a factor of 2 of the measured heating rate—the latter being from the measured non-adiabatic temperature profiles (Section 3.2). We thus conclude that models in which the solar wind is accelerated by heating from low-frequency Alfvénic turbulence are consistent with the measured density fluctuations in the solar wind. By contrast, models in which coronal holes and the near-Sun solar wind are accelerated by non-turbulent high-frequency waves (“sweeping”) are inconsistent with the measured density fluctuations at $5 R_{\odot}$ unless the ion-cyclotron waves have $k_{\perp} = 0$ to very high precision (Hollweg 2000). The key difference between the turbulent model and the sweeping model is that in the sweeping model the timescale t_d to dissipate the energy contained in small-scale ($\sim \rho_i$) fluctuations is the time t_{pr} required for waves to propagate a radial distance over which the field strength drops by a factor of ~ 2 , while in the turbulence model t_d is the cascade time at small scales, which can be much shorter than t_{pr} (Section 4.1). Thus for a fixed heating rate, the turbulent-heating model can have a much smaller energy density in small-scale fluctuations, and thus much smaller density fluctuations.

Future measurements and calculations could help clarify the relative importance of passive fluctuations and wave compressions in producing density fluctuations at different scales for different values of β . For example, the passive scalar contribution to the density fluctuations in the solar wind should be suppressed when $\beta \gtrsim 1$ because the damping rate of the passive fluctuations (slow waves and entropy modes) is larger than the cascade rate (Section 2). Thus, measurements of the density fluctuations in solar-wind epochs with large β are likely to be particularly instructive; more detailed theoretical calculations of the suppression of the passive scalar contribution at $\beta \gtrsim 1$ would aid in interpreting such measurements. In addition, future progress toward understanding the inertial-range power spectra of the density fluctuations, Sunward Alfvén waves, and anti-Sunward Alfvén waves in imbalanced (or cross-helical) turbulence could lead to significantly tighter constraints on the heating rate contributed by low-frequency Alfvén-wave turbulence, particularly near the Sun where the energy in anti-Sunward Alfvén waves greatly exceeds the energy of Sunward Alfvén waves.

Finally, we note that although our results are consistent with models in which the solar wind is heated by low-frequency Alfvén-wave turbulence, it is not yet clear whether this type of turbulence can explain the “perpendicular ion heating” (i.e., the preferential enhancement of thermal motions \perp to \mathbf{B}_0) that is observed in the corona (Kohl et al. 1998; Antonucci et al. 2000) and fast-solar wind (Marsch et al. 2004; Hellinger et al. 2006). It is also not yet clear whether low-frequency Alfvén waves launched from the Sun can cascade rapidly enough to dissipate within a few R_{\odot} of the solar surface, which is required if these waves are to explain the observation of strong ion heating close to the Sun (Kohl et al. 1998; Antonucci et al. 2000). Resolving these uncertainties will be important for determining more precisely the role of Alfvén-wave turbulence in the solar wind.

We thank Joe Hollweg for helpful discussions. This work was supported in part by DOE grant DE-FG02-07-ER46372, NSF grant ATM-0851005, NSF-DOE grant AST-0613622, and NASA grants NNX07AP65G and NNX08AH52G. E.Q. was supported in part by NSF-DOE grant PHY-0812811 and by NSF grant ATM-0752503.

REFERENCES

- Abraham-Shrauner, B., & Feldman, W. C. 1977, *J. Geophys. Res.*, **82**, 618
 Allen, L. A., Habbal, S. R., & Hu, Y. Q. 1998, *J. Geophys. Res.*, **103**, 6551
 Antonucci, E., Doderio, M. A., & Giordano, S. 2000, *Solar Phys.*, **197**, 115
 Axford, W. I., & McKenzie, J. F. 1992, in *Solar Wind Seven*, ed. E. Marsch & R. R. Schwenn (New York: Pergamon), **1**
 Bavassano, B., Pietropaolo, E., & Bruno, R. 2000, *J. Geophys. Res.*, **105**, 15959
 Beresnyak, A., & Lazarian, A. 2008, *ApJ*, **682**, 1070
 Beresnyak, A., & Lazarian, A. 2009, *ApJ*, **702**, 460
 Celnikier, L. M., Harvey, C. C., Jegou, R., Kemp, M., & Moricet, P. 1983, *A&A*, **126**, 293
 Celnikier, L. M., Muschietti, L., & Goldman, M. V. 1987, *A&A*, **181**, 138
 Chandran, B. D. G. 2005, *Phys. Rev. Lett.*, **95**, 265004
 Chandran, B. D. G. 2008a, *ApJ*, **685**, 646
 Chandran, B. D. G. 2008b, *Phys. Rev. Lett.*, **101**, 235004
 Chandran, B. D. G., & Hollweg, J. V. 2009, *ApJ*, **707**, 1659
 Chandran, B. D. G., Quataert, E., Howes, G. G., Hollweg, J. V., & Dorland, W. 2009, *ApJ*, **701**, 652
 Coleman, P. J. 1968, *ApJ*, **153**, 371
 Coles, W. A., & Harmon, J. K. 1989, *ApJ*, **337**, 1023
 Coles, W. A., Grall, R. R., & Klinglesmith, M. T. 1995, *J. Geophys. Res.*, **100**, 17069
 Cranmer, S. R., Mattheaus, W. H., Breech, B. A., & Kasper, J. C. 2009, *ApJ*, **702**, 1604

- Cranmer, S. R., & van Ballegoijen, A. A. 2003, *ApJ*, **594**, 573
- Cranmer, S. R., & van Ballegoijen, A. A. 2005, *ApJS*, **156**, 265
- Cranmer, S. R., van Ballegoijen, A. A., & Edgar, R. J. 2007, *ApJS*, **171**, 520
- Czechowski, A., Ratkiewicz, R., McKenzie, J. F., & Axford, W. I. 1998, *A&A*, **335**, 303
- Del Zanna, L., Velli, M., & Londrillo, P. 2001, *A&A*, **367**, 705
- Dmitruk, P., Matthaeus, W. H., Milano, L. J., Oughton, S., Zank, G. P., & Mullan, D. J. 2002, *ApJ*, **575**, 571
- Dmitruk, P., Milano, L. J., & Matthaeus, W. H. 2001, *ApJ*, **548**, 482
- Dobrowolny, M., Mangeney, A., & Veltri, P. L. 1980, *Phys. Rev. Lett.*, **76**, 3534
- Esser, R., Habbal, S. R., Coles, W. A., & Hollweg, J. V. 1997, *J. Geophys. Res.*, **102**, 7063
- Feldman, W. C., Habbal, S. R., Hoogeveen, G., & Wang, Y.-M. 1997, *J. Geophys. Res.*, **102**, 26905
- Fisher, R., & Guhathakurta, M. 1995, *ApJ*, **447**, L139
- Fisk, L. A. 2003, *J. Geophys. Res.*, **108**, 7
- Fisk, L. A., Gloeckler, G., Zurbuchen, T. H., Geiss, J., & Schwadron, N. A. 2003, in *AIP Conf. Ser.*, **679**, Solar Wind Ten, ed. M. Velli, R. Bruno, F. Malara, & B. Bucci (Melville, NY: AIP), 287
- Freeman, J. W. 1988, *Geophys. Res. Lett.*, **15**, 88
- Galeev, A. A., & Oraevskii, V. N. 1963, *Sov. Phys. Dokl.*, **7**, 988
- Gary, S. P., & Nishimura, K. 2004, *J. Geophys. Res.*, **109**, 2109
- Gazis, P. R., Barnes, A., Mihalov, J. D., & Lazarus, A. J. 1994, *J. Geophys. Res.*, **99**, 6561
- Goldreich, P., & Sridhar, S. 1995, *ApJ*, **438**, 763
- Grappin, R., Mangeney, A., & Marsch, E. 1990, *J. Geophys. Res.*, **95**, 8197
- Grappin, R., Pouquet, A., & Léorat, J. 1983, *A&A*, **126**, 51
- Harmon, J., & Coles, W. 2005, *J. Geophys. Res.*, **110**, A03101
- Hasegawa, A., & Chen, L. 1976, *Phys. Fluids*, **19**, 1924
- Heinemann, M., & Olbert, S. 1980, *J. Geophys. Res.*, **85**, 1311
- Hellinger, P., Trávníček, P., Kasper, J. C., & Lazarus, A. J. 2006, *Geophys. Res. Lett.*, **33**, 9101
- Heyvaerts, J., & Priest, E. R. 1983, *A&A*, **117**, 220
- Hnat, B., Chapman, S. C., & Rowlands, G. 2005, *Phys. Rev. Lett.*, **94**, 204502
- Hollweg, J. V. 1999, *J. Geophys. Res.*, **104**, 14811
- Hollweg, J. V. 2000, *J. Geophys. Res.*, **105**, 7573
- Hollweg, J. V., & Isenberg, P. A. 2002, *J. Geophys. Res.*, **107**, 1
- Hollweg, J. V., & Turner, J. M. 1978, *J. Geophys. Res.*, **83**, 97
- Hossain, M., Gray, P. C., Pontius, D. H., Matthaeus, W. H., & Oughton, S. 1995, *Phys. Fluids*, **7**, 2886
- Howes, G. G., Cowley, S. C., Dorland, W., Hammett, G. W., Quataert, E., & Schekochihin, A. A. 2008a, *J. Geophys. Res.*, **113**, A05103
- Howes, G. G., Dorland, W., Cowley, S. C., Hammett, G. W., Quataert, E., Schekochihin, A. A., & Tatsuno, T. 2008b, *Phys. Rev. Lett.*, **100**, 65004
- Iroshnikov, P. 1963, *Astron. Zh.*, **40**, 742
- Isenberg, P. A., & Hollweg, J. V. 1983, *J. Geophys. Res.*, **88**, 3923
- Kellogg, P. J., & Horbury, T. S. 2005, *Ann. Geophys.*, **23**, 3765
- Kohl, J. L., et al. 1998, *ApJ*, **501**, L127
- Kraichnan, R. H. 1965, *Phys. Fluids*, **8**, 1385
- Leamon, R. J., Smith, C. W., Ness, N. F., & Wong, H. K. 1999, *J. Geophys. Res.*, **104**, 22331
- Lithwick, Y., & Goldreich, P. 2001, *ApJ*, **562**, 279
- Lithwick, Y., & Goldreich, P. 2003, *ApJ*, **582**, 1220
- Lithwick, Y., Goldreich, P., & Sridhar, S. 2007, *ApJ*, **655**, 269
- Markovskii, S. A. 2004, *ApJ*, **609**, 1112
- Markovskii, S. A., & Hollweg, J. V. 2002a, *Geophys. Res. Lett.*, **29**, 24
- Markovskii, S. A., & Hollweg, J. V. 2002b, *J. Geophys. Res.*, **107**, 21
- Maron, J., & Goldreich, P. 2001, *ApJ*, **554**, 1175
- Marsch, E. 1991, in *Physics of the Inner Heliosphere*, ed. R. Schwen & E. Marsch (New York: Springer), 159
- Marsch, E., Ao, X.-Z., & Tu, C.-Y. 2004, *J. Geophys. Res.*, **109**, 4102
- Marsch, E., Schwenn, R., Rosenbauer, H., Muehlhaeuser, K., Piliipp, W., & Neubauer, F. M. 1982, *J. Geophys. Res.*, **87**, 52
- Marsch, E., & Tu, C.-Y. 1997, *A&A*, **319**, L17
- Matthaeus, W. H., Zank, G. P., Oughton, S., Mullan, D. J., & Dmitruk, P. 1999a, *ApJ*, **523**, L93
- Matthaeus, W. H., Zank, G. P., Smith, C. W., & Oughton, S. 1999b, *Phys. Rev. Lett.*, **82**, 3444
- McKenzie, J. F., Ip, W. H., & Axford, W. I. 1979, *Ap&SS*, **64**, 183
- Newbury, J. A., Russell, C. T., Phillips, J. L., & Gary, S. P. 1998, *J. Geophys. Res.*, **103**, 9553
- Perez, J., & Boldyrev, S. 2009, *Phys. Rev. Lett.*, **102**, 025003
- Podesta, J., & Bhattacharjee, A. 2009, *Phys. Plasmas*, submitted
- Quataert, E. 1998, *ApJ*, **500**, 978
- Quataert, E., & Gruzinov, A. 1999, *ApJ*, **520**, 248
- Richardson, J. D., Paularena, K. I., Lazarus, A. J., & Belcher, J. W. 1995, *Geophys. Res. Lett.*, **22**, 325
- Roberts, D. A., Goldstein, M. L., Klein, L. W., & Matthaeus, W. H. 1987, *J. Geophys. Res.*, **92**, 12023
- Roberts, D. A., Goldstein, M. L., Matthaeus, W. H., & Ghosh, S. 1992, *J. Geophys. Res.*, **97**, 17115
- Ruzmaikin, A., & Berger, M. A. 1998, *A&A*, **337**, L9
- Sahraoui, F., Goldstein, M. L., Robert, P., & Khotyaintsev, Y. V. 2009, *Phys. Rev. Lett.*, **102**, 231102
- Schekochihin, A. A., Cowley, S. C., Dorland, W., Hammett, G. W., Howes, G. G., Quataert, E., & Tatsuno, T. 2009, *ApJS*, **182**, 310
- Schwartz, S. J., Feldman, W. C., & Gary, S. P. 1981, *J. Geophys. Res.*, **86**, 541
- Stix, T. 1992, *Waves in Plasmas* (New York: Springer)
- Tu, C. Y., & Marsch, E. 1990, *J. Geophys. Res.*, **95**, 4337
- Tu, C. Y., & Marsch, E. 1995, *Space Sci. Rev.*, **73**, 1
- Tu, C.-Y., & Marsch, E. 1997, *Solar Phys.*, **171**, 363
- Tu, C.-Y., & Marsch, E. 2001a, *J. Geophys. Res.*, **106**, 8233
- Tu, C.-Y., & Marsch, E. 2001b, *A&A*, **368**, 1071
- Tu, C.-Y., Pu, Z.-Y., & Wei, F.-S. 1984, *J. Geophys. Res.*, **89**, 9695
- Velli, M. 1993, *A&A*, **270**, 304
- Velli, M., Grappin, R., & Mangeney, A. 1989, *Phys. Rev. Lett.*, **63**, 1807
- Verdini, A., & Velli, M. 2007, *ApJ*, **662**, 669
- Verdini, A., Velli, M., & Buchlin, E. 2009, *ApJ*, **700**, L39